

AD-A144 969

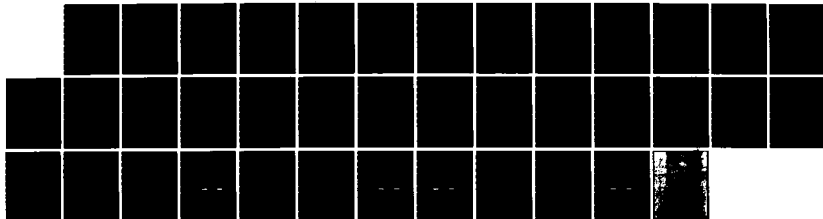
SOLUTION OF THE BOLTZMANN TRANSPORT EQUATIONS FOR A
PERMEABLE BASE TRANSI. (U) SCIENTIFIC RESEARCH
ASSOCIATES INC GLASTONBURY CT R C BUGGELN ET AL.

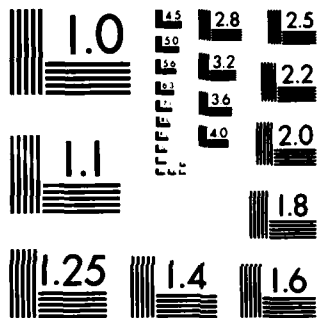
1/1

UNCLASSIFIED

20 JUL 84 SRA-R84-910005-F AFOSR-TR-84-0707 F/G 12/1

NL





MICROCOPY RESOLUTION TEST CHART
NATIONAL BUREAU OF STANDARDS-1963-A

AFOSR-TR. 84 0707

(3)

AD-A144 969

R84-910005-F

SOLUTION OF THE BOLTZMANN TRANSPORT EQUATIONS FOR A PERMEABLE BASE TRANSISTOR

by

R.C. Buggeln, J.P. Kreskovsky and H.L. Grubin
Scientific Research Associates, Inc.
P.O. Box 498
Glastonbury, CT 06033

May 1984

Prepared for:

Air Force Office of Scientific Research

Approved for Public Release; Distribution Unlimited

DTIC FILE COPY

RECEIVED
AUG 30 1984
A

84 08 30 044

Unclassified

SECURITY CLASSIFICATION OF THIS PAGE

REPORT DOCUMENTATION PAGE

1a. REPORT SECURITY CLASSIFICATION Unclassified			1b. RESTRICTIVE MARKINGS N/A									
2a. SECURITY CLASSIFICATION AUTHORITY N/A			3. DISTRIBUTION/AVAILABILITY OF REPORT Availability for Public Release Distribution Unlimited									
2b. DECLASSIFICATION/DOWNGRADING SCHEDULE N/A												
4. PERFORMING ORGANIZATION REPORT NUMBER(S) R84-910005-F			5. MONITORING ORGANIZATION REPORT NUMBER(S) AFOSR-TR-84-007									
6a. NAME OF PERFORMING ORGANIZATION Scientific Research Associates		6b. OFFICE SYMBOL (If applicable) N/A	7a. NAME OF MONITORING ORGANIZATION P.O. Box 410									
6c. ADDRESS (City, State and ZIP Code) P.O. Box 498 Glastonbury, Connecticut 06033			7b. ADDRESS (City, State and ZIP Code) P.O. Box 410 P.O. Box 410									
8a. NAME OF FUNDING/SPONSORING ORGANIZATION Air Force Office of Scientific Research		8b. OFFICE SYMBOL (If applicable) AFOSR/NE	9. PROCUREMENT INSTRUMENT IDENTIFICATION NUMBER									
8c. ADDRESS (City, State and ZIP Code) Building #41 Bolling AFB, DC 20332			10. SOURCE OF FUNDING NOS. <table border="1"><thead><tr><th>PROGRAM ELEMENT NO.</th><th>PROJECT NO.</th><th>TASK NO.</th><th>WORK UNIT NO.</th></tr></thead><tbody><tr><td></td><td></td><td></td><td></td></tr></tbody></table>		PROGRAM ELEMENT NO.	PROJECT NO.	TASK NO.	WORK UNIT NO.				
PROGRAM ELEMENT NO.	PROJECT NO.	TASK NO.	WORK UNIT NO.									
11. TITLE (Include Security Classification) Solution of the Boltzmann Transport Equation for a Permeable Base Transistor (Unclassified)												
12. PERSONAL AUTHOR(S) R.C. Buggeln, J.P. Kreskovsky, H.L. Grubin												
13a. TYPE OF REPORT Final Report		13b. TIME COVERED FROM 1983 Oct 17 TO 1984 May 31		14. DATE OF REPORT (Yr., Mo., Day) 1984 July 20								
15. PAGE COUNT 35												
16. SUPPLEMENTARY NOTATION												
17. COSATI CODES <table border="1"><thead><tr><th>FIELD</th><th>GROUP</th><th>SUB. GR.</th></tr></thead><tbody><tr><td></td><td></td><td></td></tr></tbody></table>			FIELD	GROUP	SUB. GR.				18. SUBJECT TERMS (Continue on reverse if necessary and identify by block number) Boltzmann Transport Equations, Gallium Arsenide Transistor, Permeable Base Transistor, Numerical Simulation, Alternating Direction Implicit, Linearized Block Implicit			
FIELD	GROUP	SUB. GR.										
19. ABSTRACT (Continue on reverse if necessary and identify by block number) <p>A description of a numerical method for solving the Boltzmann transport equations is presented. This numerical technique is applied to the case of the solution of the Boltzmann equations for a gallium arsenide permeable base transistor. Calculated results are presented for two base potentials.</p>												
20. DISTRIBUTION/AVAILABILITY OF ABSTRACT UNCLASSIFIED/UNLIMITED <input checked="" type="checkbox"/> SAME AS RPT. <input type="checkbox"/> DTIC USERS <input type="checkbox"/>			21. ABSTRACT SECURITY CLASSIFICATION Unclassified									
22a. NAME OF RESPONSIBLE INDIVIDUAL Dr. Gerald Witt			22b. TELEPHONE NUMBER (Include Area Code) (202)767-4931									
			22c. OFFICE SYMBOL AFOSR/NE									



1. Introduction

Considerable interest in the gallium arsenide permeable base-transistor (PBT) has developed since it was first announced by workers at MIT Lincoln Laboratories in 1979 [1]. Initial calculations indicated that large values of the unity-gain-current frequency were possible and could lead to the development of transistor amplifiers and oscillators that would operate at frequencies well into the millimeter wave frequency regime. It was also suggested that LSI/PBT logic circuits with a power-delay product less than one fJ was possible.

Since 1979, considerable work has been performed mainly at Lincoln Laboratories [2] and to a lesser extent elsewhere [3]. Workers have predicted maximum unity-current-gain frequencies as high as 80GHz for silicon as well as operating frequencies up to 30GHz for a silicon logic inverter [3]. Additionally, the operating characteristics have been shown to be sensitively dependent on the magnitude of the donor concentrations, its shape, the structure of the PBT, emitter-collecting spacing, length of the base region, etc. [4]. When one couples the expectation of superior device performance with its sensitivity to device parameters, it becomes immediately clear that the designer of a high frequency PBT is faced with a significant dilemma in choosing an optimum design. To compound these difficulties, the designer of the PBT is also faced with the dilemma that the principle design tool, numerical simulations of the PBT through solution of the semiconductor drift and diffusion equations (DDE) may not be adequate to the task. The inadequacy rests with the fact that present PBT design trends are toward submicron scales where the impact of velocity overshoot enters. The importance of velocity overshoot contributions was recognized in one of the first PBT discussions where attempts to deal with it were confined to modifications of the field dependent drift velocity [2].

While attempts at incorporating velocity overshoot effects into DDE simulations have and will continue to be useful, important design information is missing. The most critical missing element lies at the core of the nonequilibrium overshoot phenomena. Namely, that carriers do not attain equilibrium values of velocity instantaneously. Rather, there are spatial

and temporal lags - features that are absent from the DDE approach. To overcome these deficiencies newer and more fundamental approaches have been developed. One approach, simulation of the PBT through solutions to moments of the Boltzmann transport equation, was successfully implemented by workers at Scientific Research Associates, inc. (SRA) during a Phase I AFOSR/SBIR study. The purpose of this report is to summarize the Phase I study.

The report is divided into 6 sections. Section 2 is a summary of the Phase I technical objectives. Section 3 provides a brief description of the PBT and the equations used in the Phase I study. Section 4 contains a discussion of the numerical procedures. Section 5 contains the results of the study. Section 6 contains the conclusions and recommendations.

2. Phase I - Technical Goals

There were several goals of the Phase I program:

1. The principal objective was to demonstrate the feasibility of adapting an existing numerical algorithm for solving the moments of the Boltzmann transport equation (MBTE) to the study of the gallium arsenide permeable base transistor. The MBTE algorithm incorporates such key high speed and submicron features as temporal and spatial velocity overshoot. Code modification was successful and two computer runs were performed.

2. A second objective was to establish an effective program plan for utilizing the MBTE algorithm in the design and physics analysis of the PBT. A program plan was regarded as essential because the costs associated with MBTE utilization are higher than those associated with the simpler and more limited semiconductor drift and diffusion equations. The program plan developed is direct and involves two components.

1. The first component involves choosing a specific design goal, e.g., the design of a 60 and 94GHz PBT amplifier. This component utilizes drift and diffusion equation algorithms for preliminary selection of material parameters (e.g., doping variations), and device parameters (e.g., base length, emitter-collector spacings) to achieve the design goal.

- ii. The second component involves using the reduced set of parameter variations as initial input to the MBTE algorithm. The MBTE algorithm is then utilized to simulate the operation of the PBT to provide either corroboration or modifications of the DDE conclusions.

3. A third Phase I objective was to enhance an ongoing dialogue with one of the principle PBT development groups; that at MIT Lincoln Laboratories. Workers at Lincoln Laboratories have expressed a keen interest in (1) using the results of the MBTE simulations, (2) supporting part of the development necessary to bring an existing SRA/DDE algorithm on line for PBT simulations and (3) utilizing the SRA/DDE algorithm as an adjunct in both the interpretation of their experimental results and as a guide to future device design.

3. Permeable Base Transistor and the Governing Moment Equations

3a. PBT Operation

Figure 1 displays a cutaway view of the PBT where one notes the presence of an array of metallic fingers placed between two regions, labeled the emitter and collector regions. The individual metallic strips often are a composite tungsten alloy and create a Schottky barrier at the metal/semiconductor interface region. The structure of each region is identified in Figure 2, displaying an apparent similarity to that of a three-terminal field effect transistor. Indeed, the operation principles of the PBT and the MESFET are similar. (In terms of nomenclature, the following association is made between the two: emitter \leftrightarrow source, collector \leftrightarrow drain, base \leftrightarrow gate.) Apart from this similarity, there are important design advantages of the PBT over that of the FET. First, substrate injection problems associated with the MESFET are nonexistent by *design* of the PBT. Second, surface state depletion in the source-gate, gate-drain region of the MESFET is nonexistent by *design* of the PBT. Third, transport is with the exception of the base region, normal flow, thereby eliminating high current densities associated with corners of the planar FET.

The characteristic electrical properties of the PBT are in the zeroth order case its dc current-voltage characteristics at any combination of emitter-base collector-base bias level. The current flowing from the emitter to the collector reflects the channel resistance between the emitter and base, the base and collector and the enhanced resistance within the base region.

Under normally off operations the PBT is designed such that the deple-

tion region surrounding the base penetrates to the bottom of the channel minimizing the magnitude of current flow between the emitter and collector regions. Current levels increase by applying forward bias levels to the base region. Figure 3 is an illustration of the dc current-voltage relation of a normally off PBT, obtained from Reference 5. As seen from Figure 3, the PBT begins to turn on at a base threshold voltage of 0.132 volts with a collector voltage of 0.8 volts [5].

3b. Governing Equations

The operating characteristics of the PBT rests on solutions to the governing transport equations. The governing equations utilized in this study are the first three moments of the Boltzmann transport equation. These equations are derived for two different species of carriers, in this case, satellite valley and central valley carriers in gallium arsenide. The governing equations are obtained by taking the collisional invariant moments [6] of the Boltzmann transport equation, viz., the moments with respect to the mass, momentum and energy of the two carriers. This yields a set of governing equations which is similar in form to the equations utilized for two-phase fluid dynamic flow. The governing equations reflect the conservation laws of mass, momentum and energy for the two carriers and are often referred to as the moment of the Boltzmann transport equations.

Using vector notation, the two particle conservation equations can be expressed as

$$\frac{\partial n_1}{\partial t} = -\nabla \cdot (n_1 \vec{V}_1) - n_1 f_1 + n_2 f_2 \quad (1)$$

and

$$\frac{\partial n_2}{\partial t} = -\nabla \cdot (n_2 \vec{V}_2) + n_1 f_1 - n_2 f_2 \quad (2)$$

where n_1 and n_2 are the satellite valley and central valley carrier number

densities respectively while \vec{V}_1 and \vec{V}_2 are the corresponding velocities. f_1 and f_2 are the corresponding scattering integrals for mass conservation and in general are functions of the corresponding carrier temperature and momenta [6]. For the purposes of this study, the dependence of all scattering integrals on momenta is neglected. Defining a total or global number density, n , by

$$n \equiv n_1 + n_2 \quad (3)$$

and adding Eq. (1) to Eq. (2) yields the equivalent relationship, i.e., the global continuity equation

$$\frac{\partial n}{\partial t} = -\nabla \cdot [n_1 \vec{V}_1 + (n - n_1) \vec{V}_2] \quad (4)$$

Conservation of momentum for the satellite valley carrier can be expressed as

$$\frac{\partial}{\partial t}(n_1 \vec{P}_1) = -\nabla \cdot (n_1 \vec{V}_1 \vec{P}_1) - \nabla \rho_1 - \nabla \cdot \sigma_1 - n_1 e \vec{E} - n_1 \vec{P}_1 f_3 \quad (5)$$

where the momentum, \vec{P}_1 , and the electric field, \vec{E} , are defined by

$$\vec{P}_1 \equiv m_1 \vec{V}_1 \quad (6)$$

$$\vec{E} = -\nabla \psi \quad (7)$$

where m_1 is the mass of the satellite valley carrier, e is the electronic charge and ψ is the electric potential. The partial pressure, P_1 , is related to the satellite valley carrier temperature, T_1 , and number density by the perfect gas relationship

$$P_1 = n_1 k T_1 \quad (8)$$

where k is Boltzmann's constant. f_3 is the scattering integral for the

satellite valley carrier momentum. The term $\nabla \cdot \sigma_1$ represents the stress forces. In this study, the stress tensor, σ_1 , is approximated by the Stokes relationship

$$\sigma_1 = -\mu_1 (\nabla \bar{V}_1 + \nabla \bar{V}_1^T - \frac{2}{3} \nabla \cdot \bar{V}_1) \quad (9)$$

where μ is the viscosity associated with the satellite valley carriers. Substitution of Eq. (6) and Eq. (7) into Eq. (5) and dividing by m_1 yields the final form of the momentum equation for the satellite valley carriers, viz.,

$$\frac{\partial}{\partial t} (n_1 \bar{V}_1) = -\nabla \cdot (n_1 \bar{V}_1 \bar{V}_1) - \frac{\nabla \rho_1}{m_1} - \frac{\nabla \cdot \sigma_1}{m_1} + \frac{n_1}{m_1} e \nabla \psi - n_1 \bar{V}_1 f_3 \quad (10)$$

It is observed that Eq. (10) is a vector equation and hence can in general be considered as l independent equations where l is the number of relevant physical dimensions.

An analogous derivation for the central valley carriers plus the identity of Eq. (3) yields the momentum equation for that species

$$\frac{\partial}{\partial t} [(n - n_1) \bar{V}_2] = \nabla \cdot [(n - n_1) \bar{V}_2 \bar{V}_2] - \frac{\nabla \rho_2}{m_2} - \frac{\nabla \cdot \sigma_2}{m_2} + (n - n_1) \frac{e}{m_2} \nabla \psi - (n - n_1) \bar{V}_2 f_4 \quad (11)$$

where

$$\rho_2 = (n - n_1) k T_2 \quad (12)$$

and

$$\sigma_2 = -\mu_2 (\nabla \bar{V}_2 + \nabla \bar{V}_2^T - \frac{2}{3} \nabla \cdot \bar{V}_2) \quad (13)$$

m_2 is the mass of a central valley carrier and μ_2 is the corresponding viscosity

coefficient. f_4 is the scattering integral for central valley carriers and is assumed to be a function of the central valley carrier temperature, T_2 , only.

There are various forms in which the satellite valley and central valley carrier energy equations can be described. This study chooses to cast the energy equations in terms of the satellite and central valley temperatures, T_1 and T_2 . As with the momentum equation, we start with the satellite valley carrier energy equation. This equation can be expressed as a balance between the time rate of change of the total energy (internal plus kinetic energy), the convection of that energy, the pressure, stress and electrical field work, the heat conduction and the production and depletion of energy due to the change of satellite valley carriers to central valley carriers and vice versa. Mathematically, the above physical statement can be expressed as

$$\begin{aligned} \frac{\partial}{\partial t} \left[n_1 \left(m_1 \frac{\vec{V}_1 \cdot \vec{V}_1}{2} + u_1 \right) \right] = & -\nabla \cdot \left[n_1 \vec{V}_1 \left(m_1 \frac{\vec{V}_1 \cdot \vec{V}_1}{2} + u_1 \right) \right] - \nabla \cdot (\rho_1 \vec{V}_1) - \nabla \cdot (\sigma_1 \cdot \vec{V}_1) + n_1 e \nabla \psi \cdot \vec{V}_1 \\ & + \nabla \cdot (\tilde{\kappa}_1 \nabla T_1) - \frac{3}{2} k \left[n_1 T_1 f_5 - (n - n_1) T_2 f_6 \right] \end{aligned} \quad (14)$$

where U_1 is the specific internal energy of the satellite valley carriers, k_1 is the corresponding thermal conductivity and f_5 and f_6 are the scattering integrals for the satellite valley energy equation (which are again assumed to be functions of temperature only). To obtain the static temperature version of Eq. (14) requires the elimination of the kinetic terms

$\frac{(\vec{V}_1 \cdot \vec{V}_1)}{2}$ of Eq. (14) through the use of the mechanical energy equation.

The mechanical energy equation is obtained by dotting the satellite valley carrier velocity, \vec{V}_1 , with the satellite valley carrier momentum equation, applying the vector identities

$$\vec{V}_1 \cdot \nabla (n_1 \vec{V}_1 \vec{V}_1) = \nabla \cdot \left[\left(n_1 \frac{\vec{V}_1 \cdot \vec{V}_1}{2} \right) \vec{V}_1 \right] + \frac{\vec{V}_1 \cdot \vec{V}_1}{2} \nabla \cdot (n_1 \vec{V}_1) \quad (15)$$

$$\bar{V}_1 \cdot \frac{\partial}{\partial t} (n_1 \bar{V}_1) = \frac{\partial}{\partial t} (n_1 \frac{\bar{V}_1 \cdot \bar{V}_1}{2}) + \frac{\bar{V}_1 \cdot \bar{V}_1}{2} \frac{\partial n_1}{\partial t} \quad (16)$$

and the satellite valley particle conservation equation, Eq. (1)

This yields upon multiplying by m_1

$$\begin{aligned} \frac{\partial}{\partial t} (m_1 n_1 \frac{\bar{V}_1 \cdot \bar{V}_1}{2}) = & -\nabla \cdot \left[(m_1 n_1 \frac{\bar{V}_1 \cdot \bar{V}_1}{2}) \bar{V}_1 \right] - \bar{V}_1 \cdot \nabla \rho_1 - \bar{V}_1 \cdot (\nabla \cdot \sigma_1) + n_1 e \bar{V}_1 \cdot \nabla \psi \\ & + \frac{\bar{V}_1 \cdot \bar{V}_1}{2} m_1 [n_1 (2f_3 - f_1) - (n - n_1) f_2] \end{aligned} \quad (17)$$

Equation (17) is next subtracted from Eq. (14) and with the use of the vector identities

$$\nabla \cdot (\sigma_1 \cdot \bar{V}_1) = \bar{V}_1 \cdot (\nabla \cdot \sigma_1) + \sigma_1 : \nabla \bar{V}_1 \quad (18)$$

and

$$\nabla \cdot (\rho_1 \bar{V}_1) = \bar{V}_1 \cdot \nabla \rho_1 + \rho_1 \nabla \cdot \bar{V}_1 \quad (19)$$

the internal energy version of the energy equation is obtained, viz.,

$$\begin{aligned} \frac{\partial}{\partial t} (n_1 u_1) = & \nabla \cdot (n_1 \bar{V}_1 u_1) - \rho_1 \nabla \cdot \bar{V}_1 - \sigma_1 : \nabla \bar{V}_1 + \nabla \cdot (\tilde{\kappa}_1 \nabla T_1) \\ & + \frac{\bar{V}_1 \cdot \bar{V}_1}{2} m_1 [n_1 (2f_3 - f_1) - (n - n_1) f_2] - \frac{3}{2} k [n_1 T_1 f_5 - (n - n_1) T_2 f_6] \end{aligned} \quad (20)$$

It is to be noted that the electric field term has disappeared in this form of the equation; in addition, the term $\sigma_1 : \nabla \bar{V}_1$ is often called the dissipation term. Finally, to obtain the static temperature version of the satellite valley carrier energy equation, the relationship between internal energy and static temperature

$$u_1 = \frac{3}{2} k T_1 \quad (21)$$

and the equation of state, Eq. (8) must be utilized. This yields upon multiplying by $\frac{2}{3k}$ the static temperature energy equation.

$$\begin{aligned} \frac{\partial}{\partial t}(n_1 T_1) = & -\nabla \cdot (n_1 \vec{V}_1 T_1) - \frac{2}{3} n_1 T_1 \nabla \cdot \vec{V}_1 - \frac{2}{3k} \sigma_1 : \nabla \vec{V}_1 + \frac{2}{3k} \nabla \cdot (\tilde{\kappa}_1 \nabla T_1) \\ & + 3 \vec{V}_1 \cdot \vec{V}_1 m_1 [n_1 (2f_3 - f_1) - (n - n_1) f_2] - n_1 T_1 f_5 + (n - n_1) T_2 f_6 \end{aligned} \quad (22)$$

In an analogous manner the energy equation can be derived for the central valley carrier. The results are

$$\begin{aligned} \frac{\partial}{\partial t}[(n - n_1) T_2] = & -\nabla \cdot [(n - n_1) \vec{V}_2 T_2] - \frac{2}{3} (n - n_1) T_2 \nabla \cdot \vec{V}_2 - \frac{2}{3k} \sigma_2 : \nabla \vec{V}_2 + \frac{2}{3k} \nabla \cdot (\tilde{\kappa}_2 \nabla T_2) \\ & + 3 \vec{V}_2 \cdot \vec{V}_2 m_2 [(n - n_1)(2f_4 - f_2) + n_1 f_1] + n_1 T_1 f_6 - (n - n_1) T_2 f_7 \end{aligned} \quad (23)$$

where f_2 and f_8 are the scattering integrals for the central valley energy equation and κ_2 is the thermal conductivity.

The partial differential equations, Eqs. (1), (4), (10), (11), (22) and (23) with equations of state, Eqs. (8) and (12), and the constitutive relations for the stress tensors, Eqs. (9) and (13), constitute the governing equations utilized in this study. Eqs. (8), (9), (12) and (13) can be substituted into the six partial differential equations, thus relating the dependent variables utilized in this study, viz. n_1 , n , \vec{V}_1 , \vec{V}_2 , T_1 and T_2 . In addition, a governing equation must be supplied for the electric potential ψ as this term occurs in both the moment equations.

The electric potential can be related to the total number density through a Poisson's equation of the form

$$\nabla^2 \psi = \frac{e}{\epsilon} (n - N_0) \quad (24)$$

where N_0 is the doping number density (given), ϵ is the permittivity and e the electron charge. It is to be noted that the particle conservation equations, the momenta equations and the energy equations all have time (rate) terms while the Poisson's equation for electric potential has no such term. In addition, if we restrict ourselves to two-dimensional problems, it is seen that the governing partial differential equations, Eq. (1), (4), (10), (11), (22), (23) and (24) relate nine independent variables for nine equations (the momentum equations are vector equations and in two dimension are each two separate, independent equations). This governing system of equations is coupled and many of the terms are nonlinear. To solve such a system of equations requires an initial distribution of each of the independent variables as well as the various coefficients in the governing equation, e.g. κ_1 , κ_2 , μ_1 , μ_2 , etc. In addition, boundary conditions are needed to uniquely define the problem. The boundary conditions will depend on the problem considered and discussion of that matter will be deferred to Section 5 (the results section) where boundary conditions are specified for a sample problem. An equation set as complex as the governing system of equations (which will subsequently be referred to as the moments of the Boltzmann transport equations (MBTE) obviously has no closed form of solution, except for the most trivial of problems. Hence, attempts to solve this set of equations with given initial conditions and boundary conditions was accomplished by means of a numerical procedure.

4. Solution of the Governing Equations

The numerical method used in the solution of the governing equations, which were derived in the previous section, is based on an application of consistently split, linearized, block implicit (LBI) methods as developed by Briley and McDonald [7,8]. LBI methods have been highly successful in the field of computational fluid dynamics (CFD) where they have been applied in obtaining solutions to a closely related system of governing equations, the Navier-Stokes equations, [c.f. Ref. 7]. Thus, application of such methods to solution of the moments of the Boltzmann transport equation can draw on a vast amount of related experience generated using LBI techniques.

LBI techniques center about the use of a formal linearization procedure in which systems of coupled nonlinear PDE's in one space dimension are reduced to a system of linear equations, which upon application of spatial differencing, may be expressed as a block coupled matrix system. The resulting system may then be solved efficiently, without iteration, to advance the solution in time. Steady solutions are obtained as the long-time asymptotic solution. The benefits of the procedure are retained for multidimensional problems through application of ADI schemes in their natural extension to block coupled systems. The ADI procedures reduce the multidimensional system of equations, having broad-banded matrix structures to systems of one-dimensional equations with narrow block-banded structures which are solved efficiently using fundamental block-elimination methods.

Briley and McDonald [7] considered the coupled system of nonlinear, time-dependent, multidimensional equations given by

$$\frac{\partial H(\phi)}{\partial t} = D(\phi) + S(\phi) \quad (25)$$

In Eq. (25), ϕ represent the vector of dependent variables $\phi = (n_1, n_1 \vec{v}_1, \vec{v}_2 T_1 T_2, \psi)^T$, $H(\phi)$ and $S(\phi)$ are nonlinear functions of ϕ , and $D(\phi)$ is a general, nonlinear, multidimensional, partial differential operator. Equation (25) is first time differenced about $t^n + \beta \Delta t$

$$\frac{H^{n+1} - H^n}{\Delta t} = \beta(D^{n+1} + S^{n+1}) + (1-\beta)(D^n + S^n) \quad (26)$$

where $\Delta t = t^{n+1} - t^n$. The parameter $\beta = 1$ for a fully implicit scheme or $\beta = 0.5$ for the Crank-Nicolson formulation. The implicit level nonlinear operators H, D and S are then formally linearized using a Taylor series expansion about the explicit time level. For example

$$H^{n+1} = H^n + \left(\frac{\partial H}{\partial \phi}\right)^n (\phi^{n+1} - \phi^n) + \mathcal{O}(\Delta t^2) \quad (27)$$

Eq. (26) may then be expressed at each grid point in the solution domain as a matrix equation of the form

$$(A - \beta \Delta t L^n)(\phi^{n+1} - \phi^n) = \Delta t (D^n + S^n) \quad (28)$$

where

$$A \equiv \left(\frac{\partial H}{\partial \phi}\right)^n - \beta \Delta t \left(\frac{\partial S}{\partial \phi}\right)^n \quad (29)$$

and

$$L^n = \left(\frac{\partial D}{\partial \phi}\right)^n \quad (30)$$

As a result, the nonlinear, coupled system of PDE's given by Eq. (25) has been reduced to a block coupled, linear system of temporal difference equations (Eq. 28) which, upon spatial differencing, need only be solved once per time step to obtain a solution. Additionally, since the linearization error is at worst of the same order as the temporal discretization error, the linearization is not expected to introduce significant inaccuracies.

Application of Eq. (28) to second order PDE's in one space dimension, using standard three-point spatial difference approximations requires the solution of one block tridiagonal system per time step. Such a system can be solved efficiently using standard block tridiagonal elimination procedures. However, application of the LBI algorithm given by Eqs. (28-30) to multidimensional problems results in the loss of this narrow, block banded

matrix structure. The discretization of the multidimensional spatial operator results in a broad-banded matrix structure, which, if solved by direct or iterative methods, can be extremely inefficient. Such observations led Briley and McDonald [7,8] to develop consistently split LBI algorithms for multidimensional problems. The splitting is accomplished by dividing the multidimensional spatial operator, L , into one-dimensional operators associated with each coordinate direction.

$$L = L_1 + L_2 + L_3 \quad (31)$$

Eq. (28) is then split following the scalar ADI development of Douglas and Gunn [9].

$$(A - \beta \Delta t L_1^n)(\phi^* - \phi^n) = \Delta t (D^n + S^n) \quad (32a)$$

$$(A - \beta \Delta t L_2^n)(\phi^{**} - \phi^n) = A(\phi^* - \phi^n) \quad (32b)$$

$$(A - \beta \Delta t L_3^n)(\phi^{***} - \phi^n) = A(\phi^{**} - \phi^n) \quad (32c)$$

Here $\Delta\phi^*$, $\Delta\phi^{**}$ and $\Delta\phi^{***}$ are intermediate solutions of Eqs. (32a-32c). Again, if three-point operators are used to approximate the spatial operators, L_i , each of Eqs. (32a-32c) will be block-tridiagonal and can be efficiently solved. The block size and band width are independent of the number of grid points, hence the computational effort required to solve the sequence varies linearly with the total number of grid points regardless of the number of space dimensions considered. For two-dimensional problems, Eq. (32c) is omitted. Elimination of the intermediate steps in Eqs. (32a-32c) yields

$$(A - \beta \Delta t L_1^n) A^{-1} (A - \beta \Delta t L_2^n) A^{-1} (A - \beta \Delta t L_3^n) (\phi^{n+1} - \phi^n) = \Delta t (D^n + S^n) \quad (33)$$

thus

$$\phi^{n+1} = \phi^{***} + \mathcal{O}(\Delta t^3) \quad (34)$$

The development given above presents a brief outline of the LBI method used in the present investigation. A more detailed development, as well as in-depth discussion of LBI methods, the linearization procedure and related topics may be found in the article by Briley and McDonald [7].

Application of LBI procedures to Eqs. (1,4,10,11,22,23 & 24) in two space dimensions give rise to an A matrix of the form

$$A = \left[\begin{array}{cccccc|cccc} x & & & & & & 0 & & & \\ & x & & & & & 0 & & & \\ & & x & & & & 0 & & & \\ & & & x & & \bigcirc & 0 & & & \\ & & & & x & & 0 & & & \\ & & & & & x & 0 & & & \\ & \bigcirc & & & & & 0 & & & \\ & & & & & x & 0 & & & \\ & & & & & & 0 & x & 0 & \\ \hline 0 & 0 & 0 & 0 & 0 & 0 & 0 & 0 & 0 & 0 \end{array} \right] \quad (35)$$

This matrix, due to the absence of a time derivative in Poisson's equation, is singular, thus Eq. (28) cannot be split following Eq. (32). However, the partitioning of the A matrix indicated by the dotted lines in Eq. (35) suggests that if the L matrix (the linearized D-operator) could be similarly partitioned, Poisson's equation could be decoupled from the rest of the system. The remaining coupled equations could then be solved by a direct application of the LBI method outlined, followed by the solution of Poisson's equation, completing a time step. To accomplish the decoupling of Poisson's equation, it is only necessary to lag the electric field terms (the potential gradient) which appear in the momentum equations. While this formally reduces the accuracy of the temporal integration to

$O(\Delta t)$, it does not adversely effect the stability of the solution algorithm. A similar procedure has been employed by Kreskovsky and Grubin [10] in solving the semiconductor drift and diffusion equations. Solution of Poisson's equation is performed using a scalar ADI procedure with cycled acceleration parameters [7, 10]. The overall solution algorithm proceeds as follows:

- 1) Initial and boundary conditions are specified for all variables throughout the computational domain.
- 2) The continuity, momentum and energy equation are solved using an LBI scheme to advance the carrier densities, velocities and temperatures from time t^n to time $t^{n+\Delta t}$.
- 3) Poisson's equation is solved, using the carrier densities at time $t^{n+\Delta t}$, to obtain the advanced time potential distribution.
- 4) Steps 2 and 3 are repeated until a steady solution is reached or until the calculation is terminated.

Finally, a few words with regard to the spatial difference approximation and computational mesh are in order. The difference approximations used were developed for arbitrary grid spacing in either coordinated direction. Standard, conservative three-point approximations were used to assure that the fluxes of momentum, energy and current were rigorously concerned on the finite difference mesh. The actual mesh distribution can be generated manually or analytic transformations such as that of Oh [11], can be used to cluster grid points where higher resolution is required.

5. Results

The preceding analysis was incorporated into a computer program and the resultant program was used to calculate the steady state solution of the above governing equations for a gallium arsenide permeable base transistor at two separate base potentials. The results were then compared with comparable results obtained by solving the drift and diffusion equations as reported by Bozler and Alley [2]. A schematic of the gallium arsenide device investigated is shown in Fig. 1. n type emitters and collector layers are used. The base is patterned thin film tungsten while an n^+ substrate is utilized. Electrons flow from the emitter region through the tungsten grating into the collector region. The spacing between the tungsten bases is 2000 \AA and the bases have a thickness of 200 \AA . The distance between the emitter and collector is $1.02 \mu\text{m}$. The tungsten grating forms a Schottky barrier and with the insulating gallium arsenide controls the flow of the electrons from the emitter to the collector.

For the purpose of this investigation, an infinite bank of the tungsten gratings is assumed, hence planes of symmetry exist on the lines passing through the center of each gate and at a point half-way between each gate. Thus, it is possible to perform the calculation in the computational domain shown in Fig. 4. The boundary conditions used in these computations are noted on Fig. 4. On the planes of symmetry (surfaces 3) the symmetry conditions are imposed, viz. that the first derivative of all variables except normal velocity are zero. The normal velocity components are set to zero. On surface 1, the emitter contact surface, the tangential velocity components are assumed to be zero as is the central valley normal velocity component. The second derivative of the satellite valley normal velocity component is set to zero. Finally, the central valley number density and the total number density are set to their initial values (to be subsequently discussed).

On surface 2, the collector contact, all variables are extrapolated, i.e. second derivations are set to zero, except for the electric potential

which is specified at a value $V_{ce} = 1.0$ volts. On the surfaces of the embedded gate, surfaces 4 and 5, all normal components of velocity are set to zero (no penetration of the surface) while the first derivative of the tangential velocity components are set to zero (this yields a slip tangential velocity on the surfaces). For the temperature the adiabatic condition is set for both T_1 and T_2 , i.e. the first derivatives of temperature are set to zero. In addition, the first derivatives of the number densities n_1 and n are set to zero. The potential on the embedded gate is set equal to a constant whose value is

$$\psi = -\left[\phi_{BN} - \frac{E_g}{2q}\right] - \frac{KT}{q} \left(\ln \frac{N_D}{n_i}\right) + V_{BE} \quad (36)$$

where ϕ_{BN} is the Schottky-barrier height (set to 0.8 volts), E_g is the band gap energy, T is the ambient temperature (set to 300°K), N_D is the n-type impurity concentration (set to $10^{16}/\text{cm}^3$), n_i is the intrinsic electron concentration and V_{BE} had values of 0 and 0.3 volts for case I and II respectively.

Since this study was limited to the steady state solution of the governing equations transient accuracy was not necessary. Thus, any initial condition that would allow for the steady state solution to be obtained was acceptable. The technique used for this study was to initially set the values of all velocity components equal to zero (quiescent flow) and to set the values of the satellite valley and central valley temperatures equal to the reference temperature, 300°K . The global number density, n , was set equal to the reference value and the satellite valley number density was calculated from the quiescent flow equilibrium values, viz., by using the definition of total nondimensional number density, n , of unity and neglecting the temporal and convection terms in the central valley species equation to obtain

$$n_1 f_1 = n_2 f_2 \quad (37)$$

Initially, the electric potential was set by solving Poisson's equation with zero space charge. For these calculations, the values of the viscosity and thermal conductivity were assumed to be constant and were assigned values of $6.1034 \times 10^{-11} \frac{\text{gm-cm}}{\text{sec}}$ and $2.07 \times 10^{-5} \frac{\text{joules}}{\text{sec } ^\circ\text{K}}$ respectively. The effective masses of the central valley and satellite valley carriers, m_1 and m_2 were $2.0223 \times 10^{-28} \text{ gm}$ and $6.1034 \times 10^{-29} \text{ gm}$ respectively. The permittivity ϵ was chosen as $9.8 \times 10^{-13} \frac{\text{coulombs}}{\text{joule-cm}}$. The above values were chosen as being representative values for gallium arsenide.

To demonstrate the capability of the computer code associated with the above analysis, two cases were run corresponding to base potentials of 0.0 and 0.3 volts, henceforth to be referred to as Cases I and II respectively. For Case I, two separate finite difference grid structures were used to demonstrate grid independence, i.e., that the converged solutions for two separate grid structures are essentially identical. For Case II only one grid structure was used. The strategy for obtaining converged solutions for both cases was the same: (1) to take a time step as large as possible (i.e. as large as possible while maintaining a stable solution) to obtain the basic solution and (2) after the basic solution is obtained, to take successively smaller time steps to eliminate the remaining errors and thus to sharpen up the solution. If one looks at the Fourier error analysis of the governing difference equations, the taking of the large time step eliminate errors associated with the low frequency components while the taking of small time steps can be associated with the elimination of errors associated with the high-frequency components. A physical interpretation is that the taking of the large time step allows the originally quiescent solution to develop its basic features. Although the taking of such a large time step will not give temporal accuracy, this is, of no concern as the steady state converged solution is the desired end. The use of the smaller time step allows the finer features of the solution to be obtained. The above can be seen by observing the right-hand sides of the linearized difference equations. (From an iterative point of view, it is the right-hand sides of the set of linearized difference equations, or as it is sometime referred to, as the residual, that we are attempting to drive to zero at which time the steady state solution can be said to be obtained). Initially, the residuals are zero, but the imposition of the electric potential results in the movement of carriers, thus resulting in the growth of the residuals. As the basic

features of the solution develop, the residuals become larger after which the residuals will decrease to some non-negligible level. This corresponds to the elimination of the low frequency error. If one were to continue to take the same large time steps, the residuals would cease decreasing and in fact this criterion is used to determine when one stops using the large time steps. At this point, the time steps are decreased and the residuals will again start decreasing. This corresponds to the elimination of the higher frequency errors and this process is continued until the residuals reach some arbitrarily set negligible value. Usually, one can observe the solution and it will be seen that as the time steps are successively decreased, there is a point at which the solution for all practical purposes ceases to change. It is at this point, that the solution is deemed to be converged and the calculation is terminated.

For Case I, two different grid structures were utilized, Case Ia and Ib respectively. Because of the geometry associated with the permeable base transistor, a cartesian coordinate system was used. Grid point distributions were specified by the method of Oh [11]. This method allows the grid points to be specified by the use of a sum of error functions. The advantage is that each error function is centered about some point and if the appropriate wave lengths and amplitude constants are chosen, the effect of that particular error function will be limited to a small region. Thus, one has the ability of concentrating grid points in desired regions while using fewer grid points in other regions. As used in this study, relatively large numbers of grid points were used in regions where it was expected to have large gradients of the dependent variables. This procedure allows for adequate resolution of these variables in these regions. The first grid distribution used for Case Ia had 21 grid points between the axis of symmetry and 51 grid points between the emitter and collector plates. The grid distribution utilized for Case Ib used the same 21 grid points between the axis of symmetry and 63 grid points between the plates. For both cases the grid points were concentrated in the region of the base (from the streamwise or X-direction perspective) and in the region of the top of the base (from the transverse or Y-direction perspective). For Case II the same grid point distribution was used as for Case Ib.

Converged solutions were obtained for Cases 1a and 1b in 350 time steps. It was noted that during the convergence process, the satellite valley temperatures became as high as 8 times the reference temperature of 300°K . However, for the converged solution, the maximum satellite valley temperature stabilized at approximately 2.5 times the reference temperature. It was found that the maximum number of time steps taken for this case were at least an order of magnitude lower than for the comparable maximum time step allowable when the base did not exist. Examination of the reason for this was seen to be caused by the existence of the relatively large ADI splitting error (see for example ref. 7 for a discussion of ADI splitting error) in the region of the re-entrant corner of the base. Since similar phenomena have been observed in fluid dynamics calculations with re-entrant corners, this phenomenon was not unexpected [7]. Since the splitting error is proportional to the time step squared, Δt^2 , the splitting error can usually be controlled by taking a smaller time step. This was the technique used in the Phase I study. The penalty to be paid in taking small time steps is the use of more time steps (and hence more computer time) to obtain a converged solution. For case 1b, the CPU time (on the University of Minnesota Cray-1 computer) is 5.4×10^{-3} seconds per grid point per time step for nine equations. For case 1b this corresponds to approximately 2,500 seconds (approximately 42 minutes) of CPU time.

For the Case II computations, the converged solution for Case 1b was used as an initial condition. As in case 1b, a converged solution was obtained for Case II in 350 time steps. Again, the splitting error necessitated the taking of a smaller time step than would have been necessary for the case without the base region. Since the gradients are larger in the region of the base when the base voltage is increased, this case had correspondingly larger splitting error for the same time step as was used for Case 1b. Thus, an even smaller time step had to be used.

The results of the calculation are displayed as contour plots. For the case of 0.0 volts on the base contact, the potential contours are shown in Figure 5. It is noteworthy that the largest potential gradient along the line of symmetry within the channel occurs immediately downstream from the base contact. The highest electric field within this region is approximately

40kV/cm. Within the framework of the drift and diffusion equations this would tend to fix the mean carrier velocity at 1.0×10^7 cm/sec and assure that well over 90% of the Γ valley carriers had transferred to the satellite valleys. The percentage of Γ valley carriers along the line of symmetry arising from solutions to the moment equations is displayed in Figure 6. It is apparent that considerably less transfer has occurred than that associated with the drift and diffusion approximation. Indeed, the mean carrier velocities within the channel are higher than those associated with the equilibrium field dependent drift velocity, and at certain points exceed 4×10^7 cm/sec., Fig. 7. The density contours for this case are shown in Fig. 8 and these contours, as well as those of Fig. 5 are noteworthy for their similarity to those of Reference 2. It may be stated that while the carrier and potential contours are similar, the distributions of carriers between the central and satellite valleys are different from those using the drift and diffusion equations.

While it is unlikely that a full range of dc current - voltage characteristics will yield similar results using the moment equation algorithms, and the drift and diffusion algorithms, if they do, the question arises as to the usefulness of extracting high frequency device performance characteristics from dc characteristics.

The results for the forward bias calculations are shown in Figs. 9-11. For this case, the field distribution downstream from the base contact is somewhat lower than that of Figs. 5 and 8 and the magnitude of electron transfer is muted compared to zero applied base contacts. The distribution of carrier density along the channel is displayed in Fig. 10 and the remarks concerning the comparative results obtained with the drift and diffusion code are the same as that associated with Fig. 6.

6. Conclusions and Recommendations

The analysis performed under the Phase I, AFOSI/SBIR study demonstrates that a recently developed algorithm can be successfully applied to examining the electrical characteristics of the gallium arsenide permeable base transistor. The study indicates that there is a possibility for the

dc characteristics as obtained by drift and diffusion equation algorithms to be similar to those obtained using the moment equation algorithms. However, the carrier and velocity distribution will be different, and predictions based on the drift and diffusion algorithms are likely to be of limited value for high frequency operation.

While the Phase I study demonstrated the feasibility of using the moment equation algorithm for PBT study, additional algorithm development is required to improve convergence rates, particularly in the vicinity of the base.

References

1. C.O. Bozler, G.D. Alley, R.A. Murphy, D.C. Flanders and W.T. Lindley, in Proc. 7th Bien. Cornell Conf. on Active Microwave Semiconductor Devices, (1979).
2. C.O. Bozler and G.D. Alley, IEEE Trans. Electron Devices, ED-27, 1128 (1980).
3. D.E. Snyder and R.L. Kubena, IEDM Technical Digest, 612 (1981).
4. T.W. Tank, L. Sha and D.H. Navon, (To be published).
5. C.O. Bozler and G.D. Alley, Proc. IEEE, 70, 46 (1982).
6. H.L. Grubin, D.K. Ferry, G.J. Iafrate and J.R. Barker, VLSI Electronics (ed. N. Einspruch), 3, Academic Press, N.Y. (1982).
7. W.R. Briley and H. McDonald, J. Comp. Phyx. Vol. 34, 54 (1980).
8. W.R. Briley and H. McDonald, J. Comp. Phys. Vol. 24, 372 (1977).
9. J. Douglas and J.E. Gunn, Numerische Mathematik, Vol. 6, 428 (1964).
10. Kreskovsky, J.P. and Grubin, H.L., Proceeding of the Third International Conference on Numerical Analysis of Semiconductor Devices and Integrated Circuits, Galway, Ireland, June, 1983, pp. 155-160.
11. Oh, Y.H., School of Engineering Old Dominion University (1978).

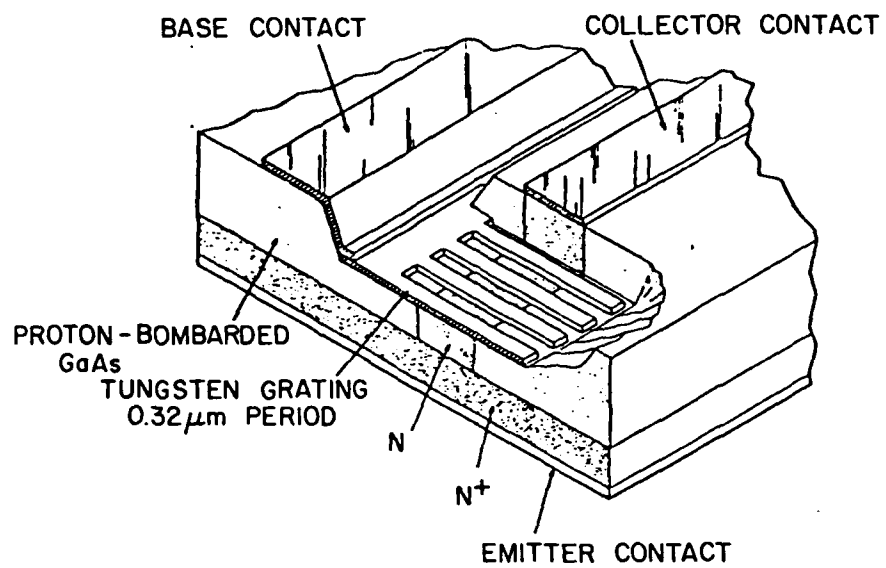


FIGURE 1. SCHEMATIC OF GaAs PBT

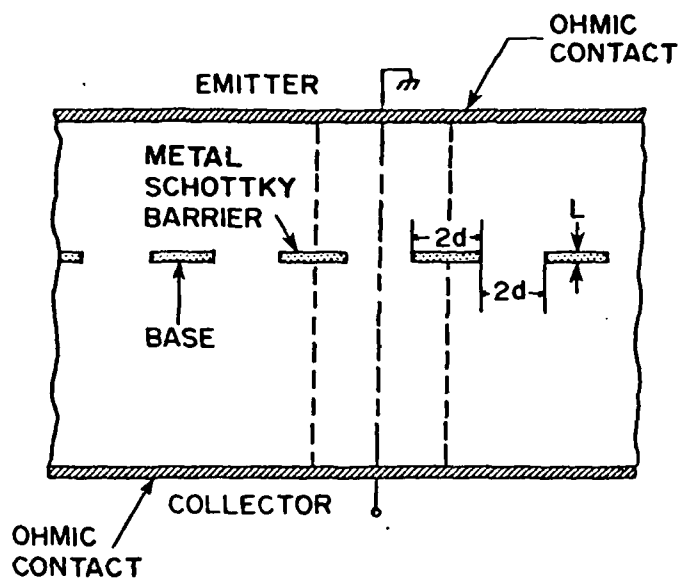


FIGURE 2. GaAs PBT DEVICE GEOMETRY

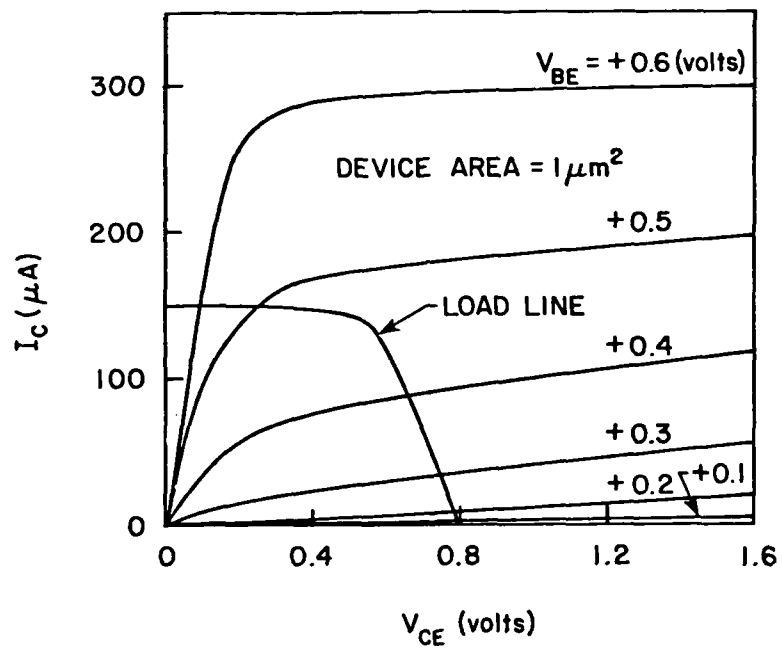
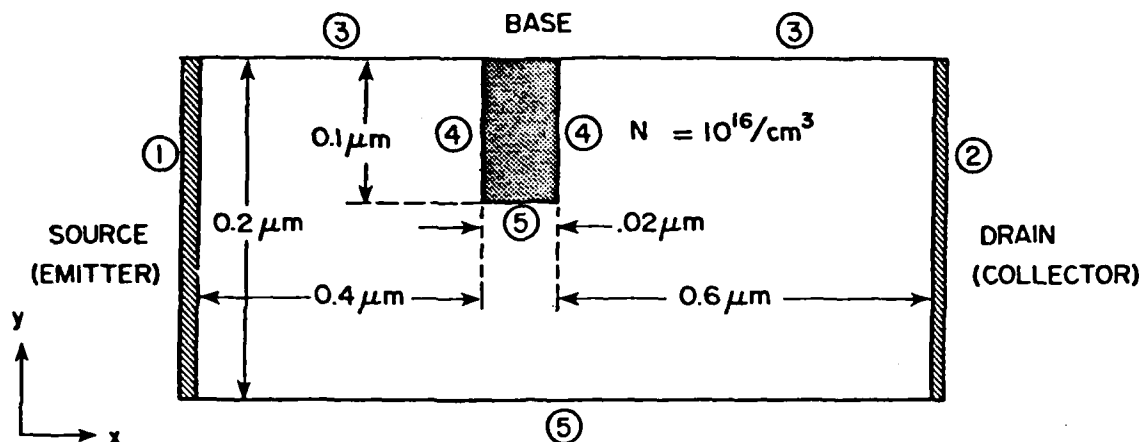


FIGURE 3. GaAs PBT COLLECTOR CHARACTERISTICS
(from Ref. 5)



SURFACE NUMBER

BOUNDARY CONDITIONS

①

$$u_1 = v_1 = v_2 = 0, \quad T_1, T_2, n_1, n \text{ specified}$$

$$\partial^2 u_2 / \partial x^2 = 0, \quad \psi = 0$$

②

$$\partial^2 \Phi / \partial x^2 = 0, \quad \Phi \text{ all variables except } \psi = V_{CE} = 1.0$$

③

$$\partial \Phi / \partial y = 0, \quad \Phi \text{ all variables} - \text{symmetry condition}$$

④

$$u_1 = u_2 = 0, \quad \partial \Phi / \partial x = 0 \quad \Phi \text{ all remaining variables}$$

$$\psi = - \left[\phi_{BN} - \frac{E_g}{2q} \right] - \frac{KT}{q} \ln \left(\frac{N_D}{n_i} \right) + V_{BE}$$

⑤

$$v_1 = v_2 = 0, \quad \partial \Phi / \partial y = 0, \quad \Phi \text{ all remaining variables}$$

$$\psi = - \left[\phi_{BN} - \frac{E_g}{2q} \right] - \frac{KT}{q} \ln \left(\frac{N_D}{n_i} \right) + V_{BE}$$

u is x direction velocity; v is y direction velocity.

FIGURE 4. COMPUTATIONAL DOMAIN WITH BOUNDARY CONDITIONS

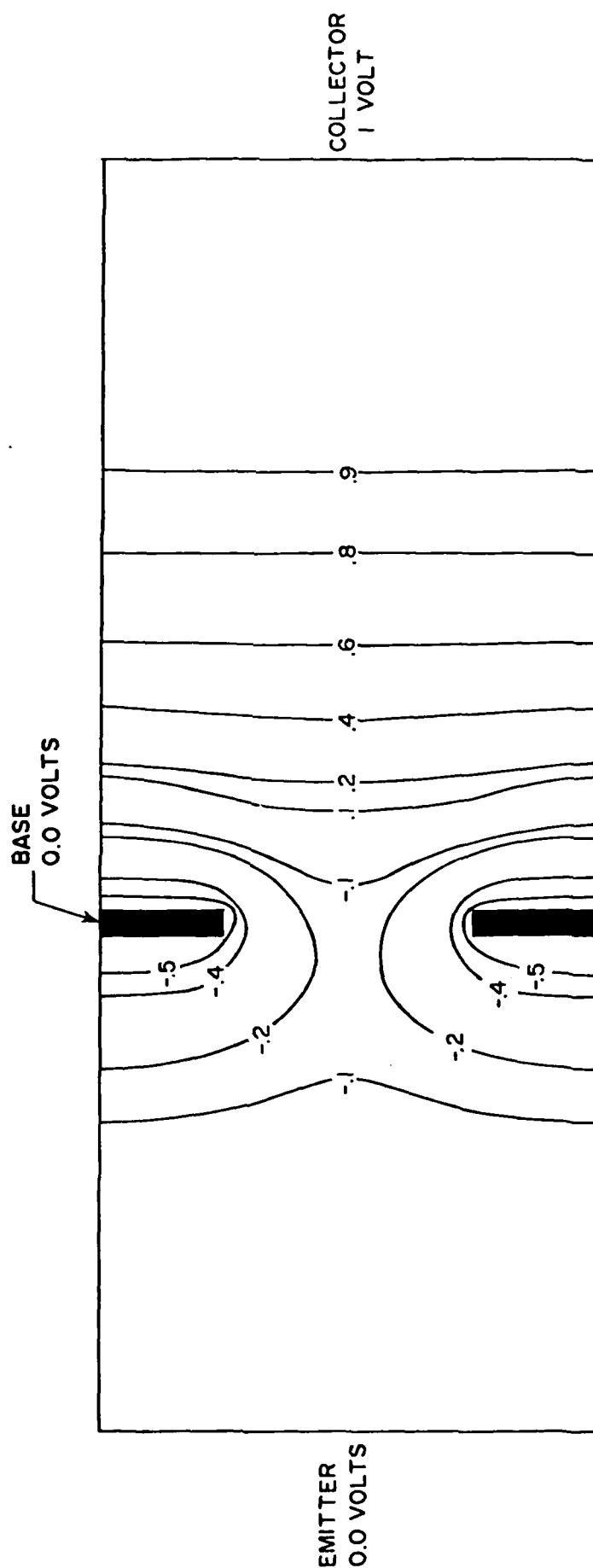


FIGURE 5. CONTOURS OF POTENTIAL (volts) - BASE 0.0 volts

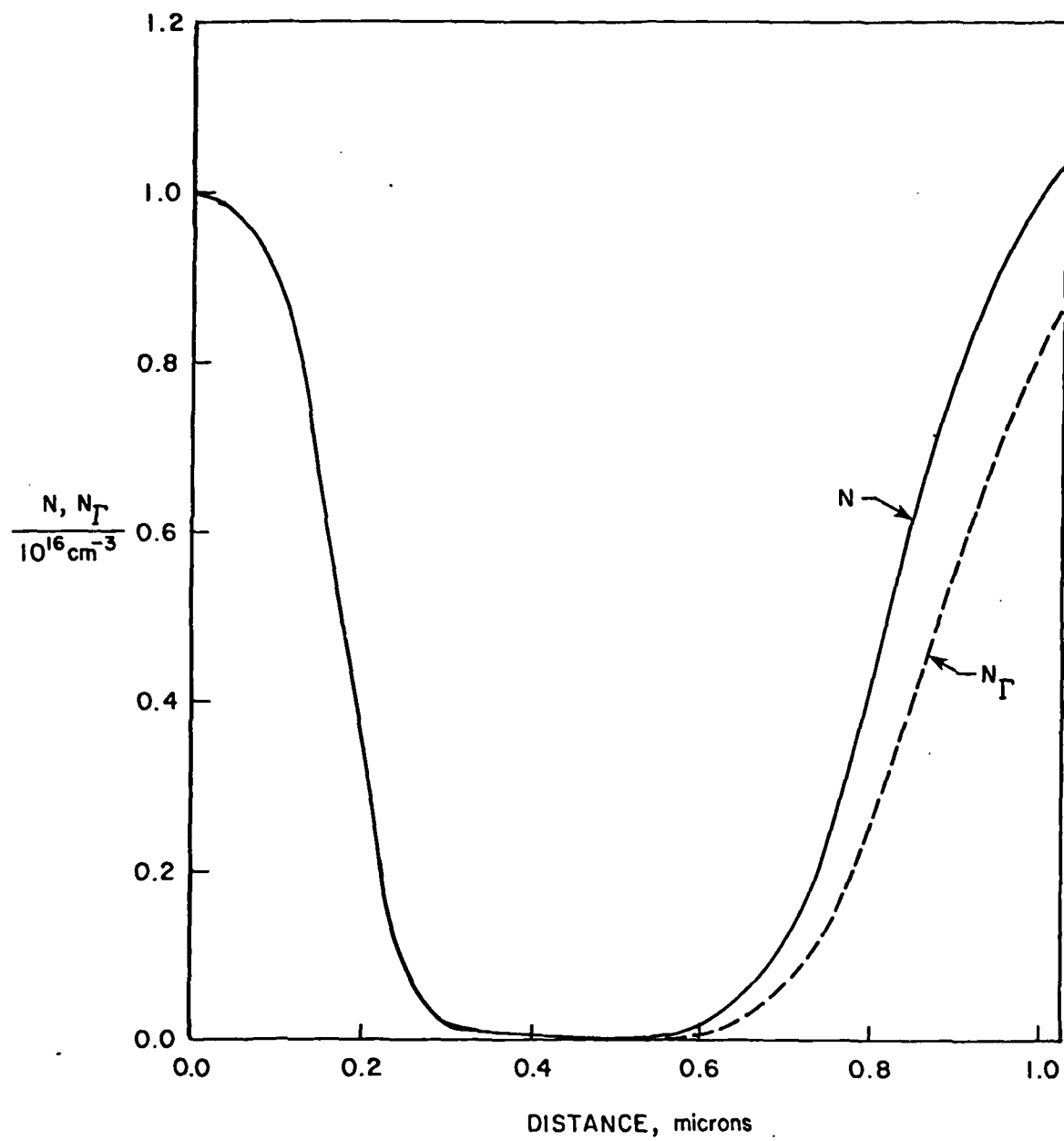


FIGURE 6. CENTERLINE PROFILE OF N and N_T — BASE 0.0 volts

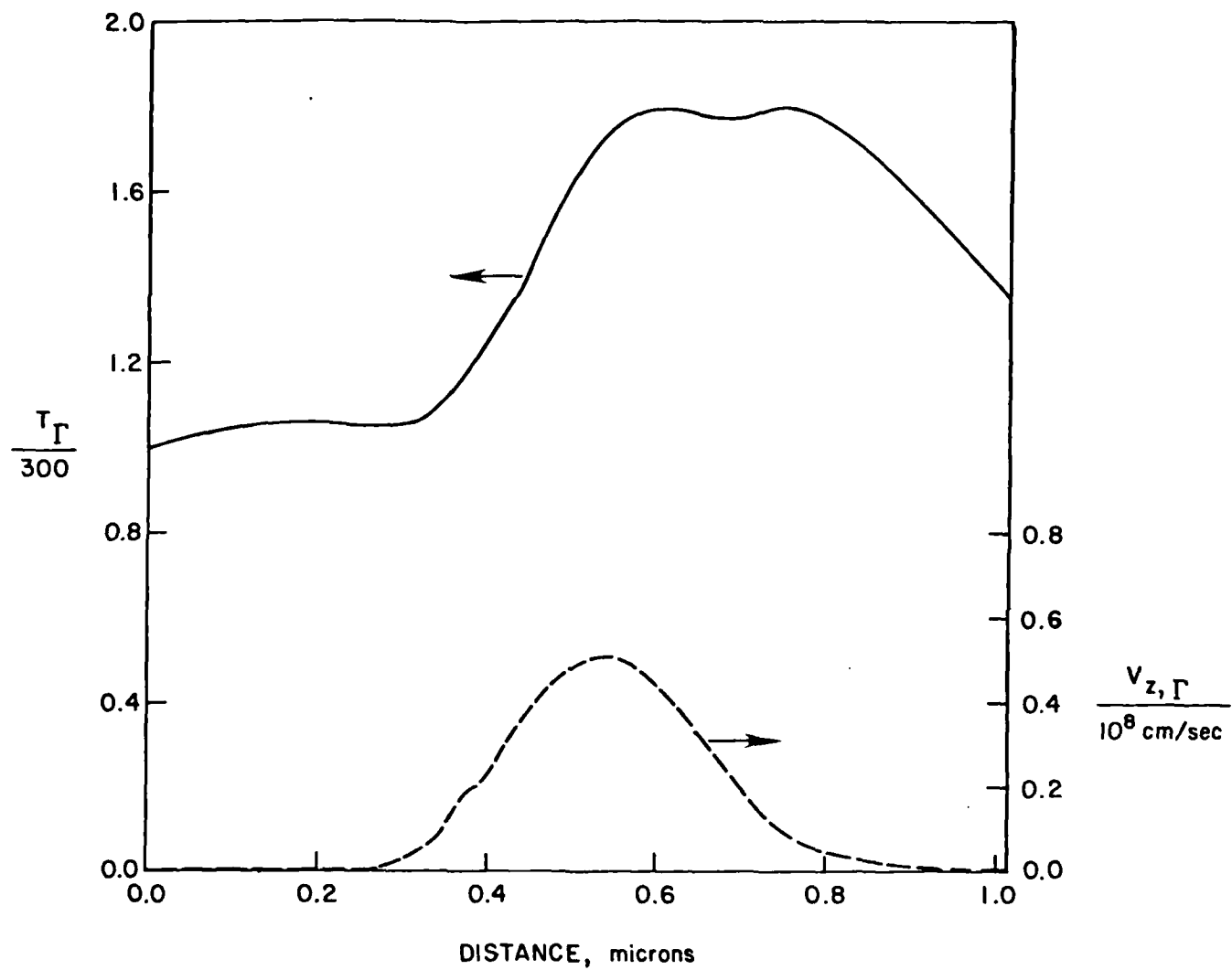


FIGURE 7. CENTERLINE PROFILE OF T_{Γ} and $V_{z,\Gamma}$ - BASE 0.0 volts

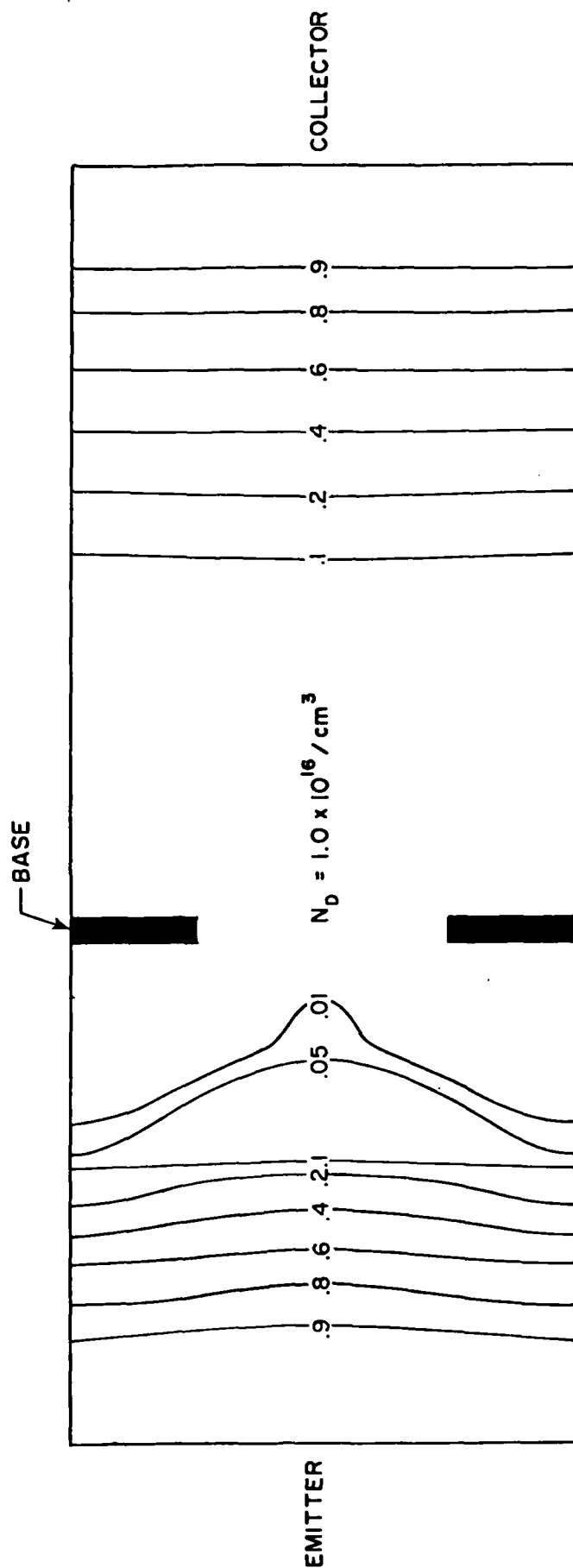


FIGURE 8. CONTOURS OF CARRIER DENSITY - BASE 0.0 volts

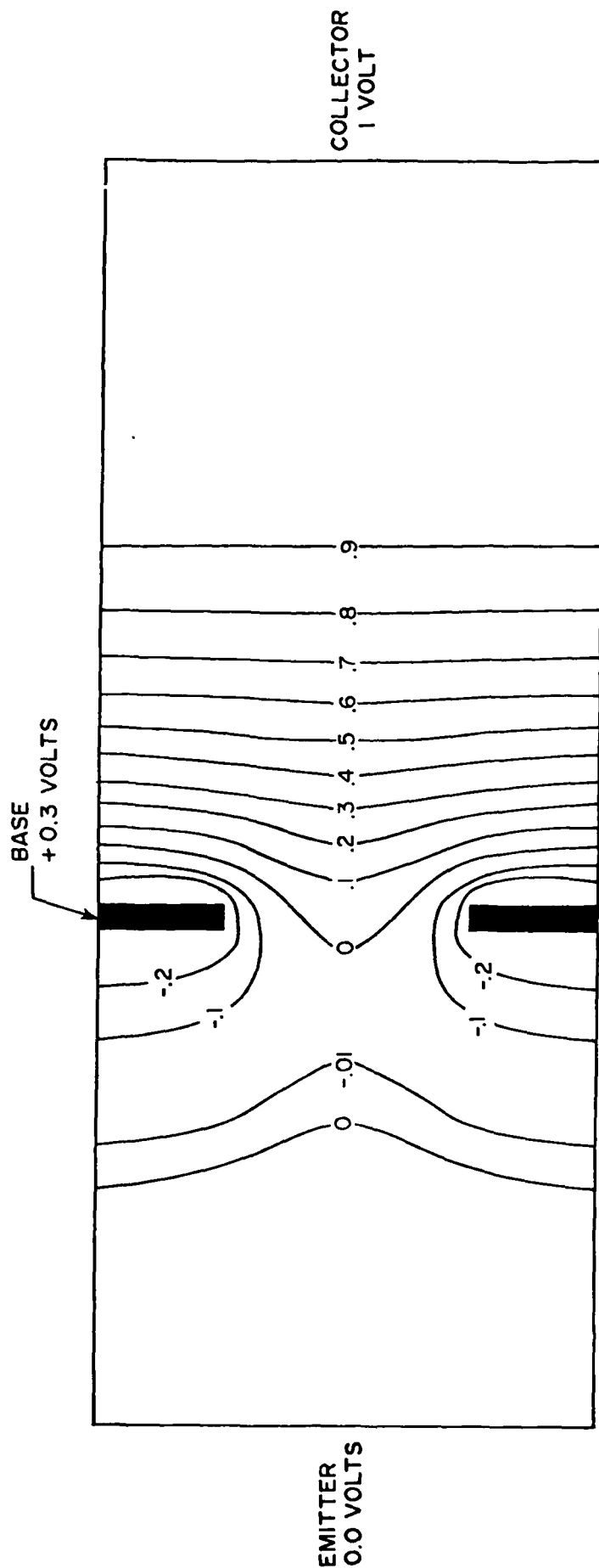


FIGURE 9. CONTOURS OF POTENTIAL (volts) — BASE 0.3 volts

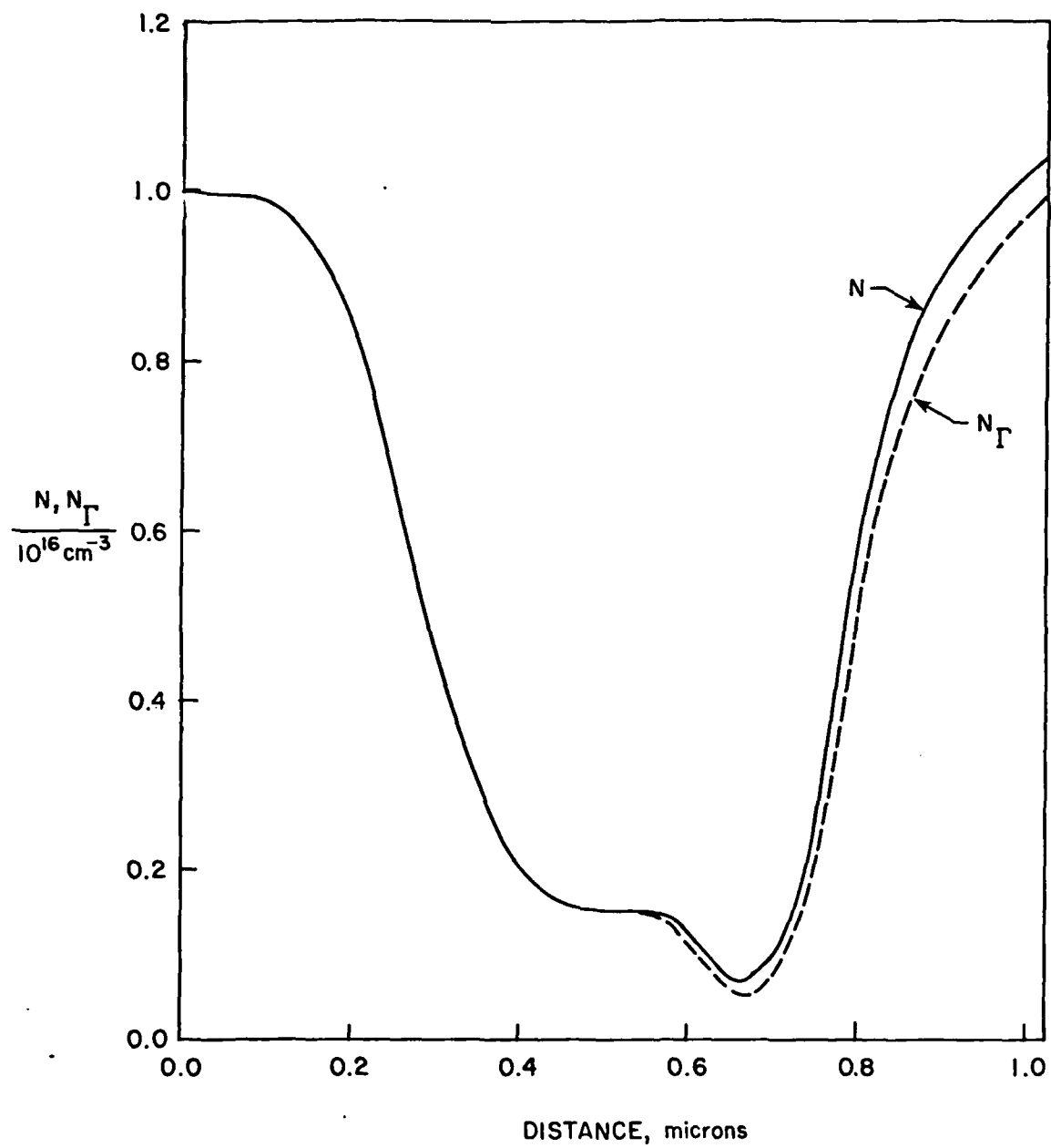


FIGURE 10. CENTERLINE PROFILE OF N and N_T — BASE 0.3 volts

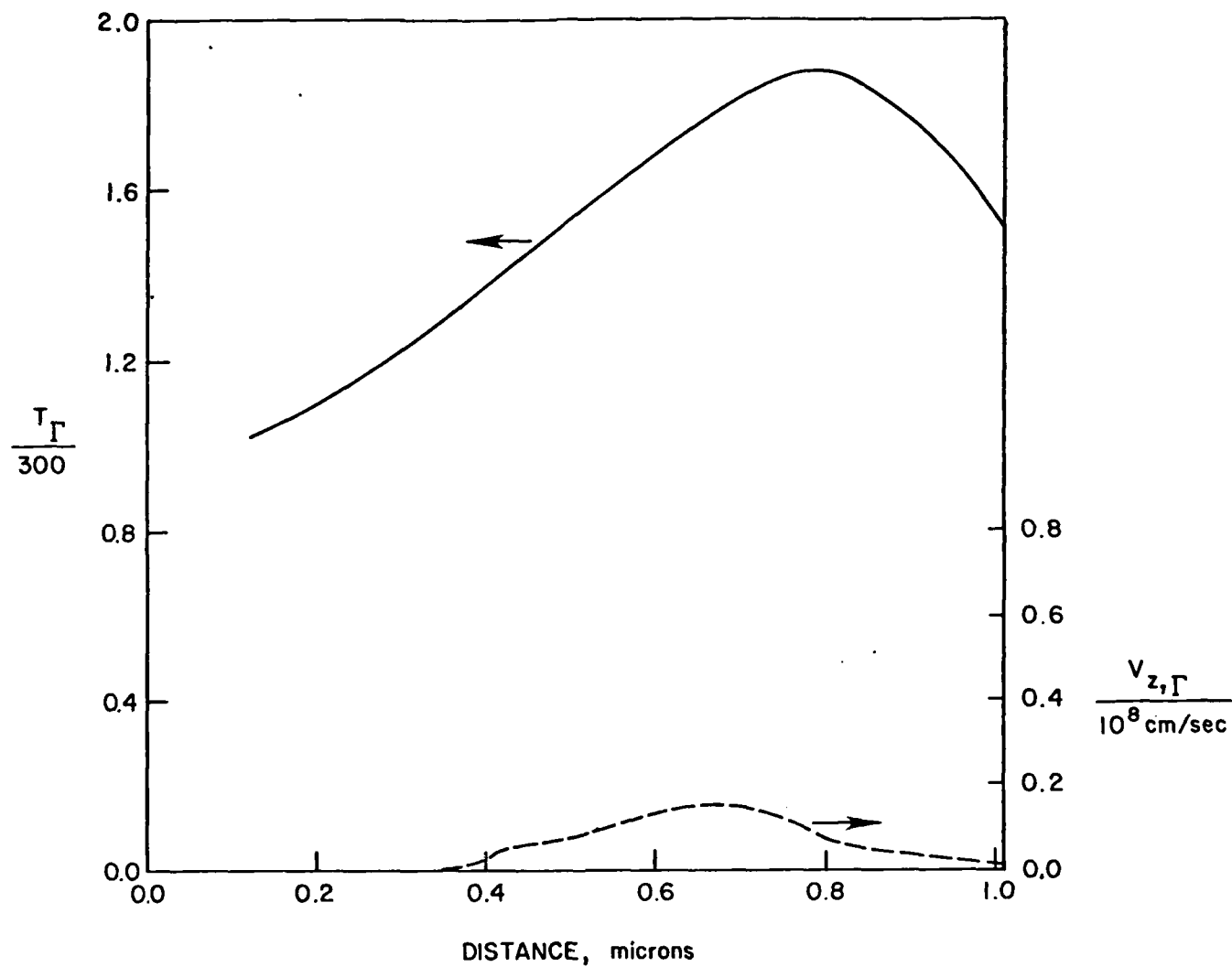


FIGURE II. CENTERLINE PROFILE OF T_{Γ} and $V_{z,\Gamma}$ - BASE 0.3 volts

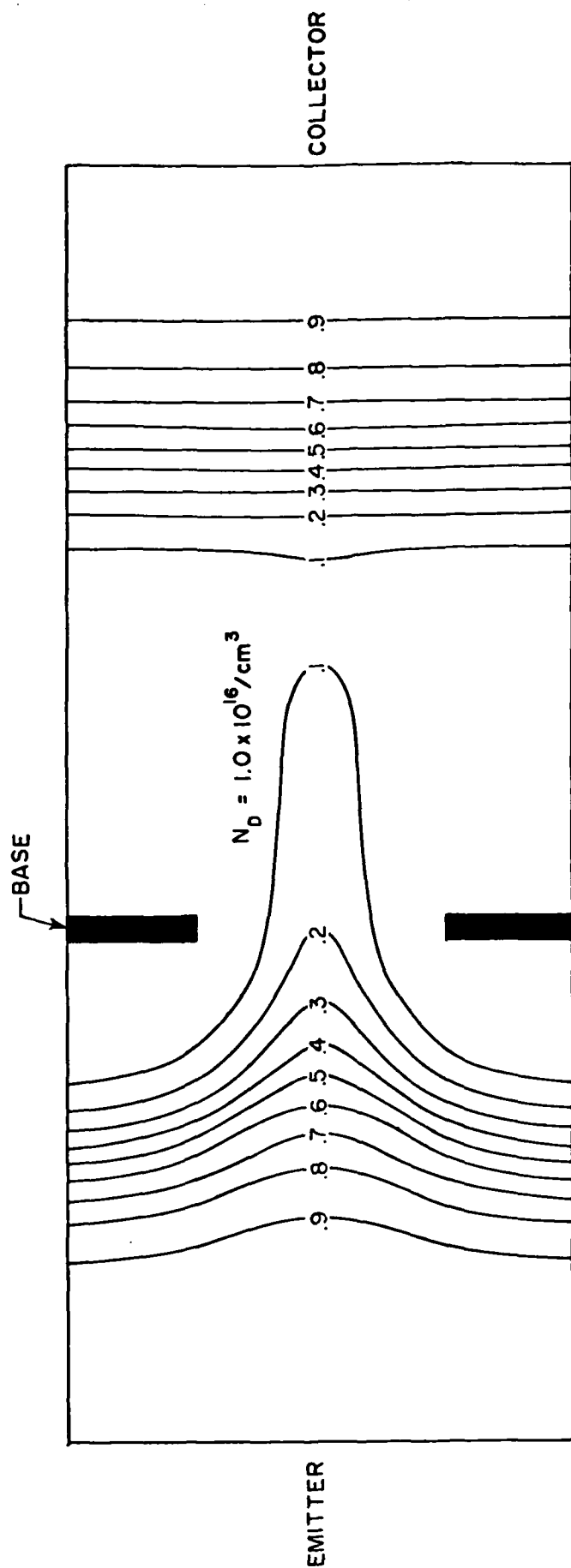


FIGURE 12. CONTOURS OF CARRIER DENSITY -- BASE 0.3 volts

END

FILMED

9-84